JOURNAL OF GUIDANCE, CONTROL, AND DYNAMICS
Vol. 19, No. 4, July–August 1996

Active Control of Flexible Structures by Use of Segmented Piezoelectric Elements

J. Callahan* and H. Baruh†
Rutgers University, Piscataway, New Jersey 08855-0909

We use segmented piezopolymer (polyvinylidene fluoride) and piezoceramic (lead zirconate titanate) materials to sense and control structural vibration to eliminate undesired elastic motion. We use modal control techniques to generate the control inputs. The elements can be of any shape or size, making control implementation simpler than for modal sensors and actuators, which must be cut into specific shapes. We analyze the performance of piezoceramic and piezopolymer materials with regard to the size of the elements and the maximum amount of charge that can be applied to the actuators. The proposed modal control method is versatile and easy to implement. System simulations on plate elements show that piezoceramic actuators are desirable for control of elastic motion.

I. Introduction

OVER the past few years, a new technology has emerged for modeling, analysis, and control of structures. This technology is that of smart structures and smart controls. These advances were made possible by the development of new materials that are manufactured as thin layers and can be used as distributed sensors and actuators. These materials convert their deformations into electrical signals that are proportional to the strain. Also, when supplied with an electrical signal, these materials deform, which generates forces and moments when they are bonded to other materials. Hence, layers of such materials can be embedded between or applied to the outside of existing composite structures for use as sensing and actuating devices. The attractiveness of such materials is obvious from the interest they have generated in recent years.[1–8] They make it possible to measure and reliably provide control inputs to any part of the structure with ease, but without adding any significant weight.

We take advantage of this technology to propose a versatile and easy-to-design control system for eliminating the elastic motion of structures. Because piezoelectric films are lightweight, more of them can be used without significantly affecting the structure to which they are applied. This leads to a larger number of possible measurements and control inputs. One approach is to design piezoelectric sensors and actuators sensitive to individual modes only.[2,6] Commonly called modal sensors and actuators, transducers of this type take advantage of the orthogonality properties of the eigenfunctions of a structure. They can be designed independently for each mode by cutting the sensors and actuators into specific shapes. Although this approach is appealing, the requirement to cut them into specific shapes may not be feasible, especially for a structure with some complexity or whose mass and stiffness properties change. Also, because more than one mode needs to be controlled, the controller for each mode needs to be stacked, which is undesirable. Our approach is to use segmented actuators of arbitrary shape, usually rectangular, to accomplish the control. No stacking of actuators is necessary.

II. General Two-Dimensional Laminated Plate

A linear piezoelectric plate theory that incorporates the piezoelectric effect into the classic laminate constitutive equations has been formulated by Lee.[9] For a thin laminate, the displacements of any point are characterized by the deformation of the geometric midplane. If the in-plane displacements (u_0, v_0) are assumed negligible as compared to the transverse deflection (w) and the output signal is generated by deformation only, then the charge $q_k(t)$ generated by each piezoelectric lamina is approximated by

$$q_k(t) = -\bar{z}_k \iint_A \left\{ F^s(\mathcal{P}) P_0(\mathcal{P}) L_w[w(\mathcal{P}, t)] \right\}_k \mathrm{d}A(\mathcal{P}) \qquad (k \in N) \quad (1)$$

where A is the plate surface domain and $\mathcal{P}$ denotes the spatial coordinates. For a rectangular plate, $\mathrm{d}A = \mathrm{d}x\,\mathrm{d}y$ and $\mathcal{P} = x, y$; for a circular plate, $\mathrm{d}A = r\,\mathrm{d}r\,\mathrm{d}\theta$ and $\mathcal{P} = r, \theta$. Equation (1) is known as the general two-dimensional sensor equation. Here, $P_0(\mathcal{P})$ accounts for polarity variations in the material. We consider piezofilms with uniform polarization $P_0(\mathcal{P}) = 1$. In Cartesian coordinates, the operator L_w has the form

$$L_w = e_{31}^0 \frac{\partial^2}{\partial x^2} + e_{32}^0 \frac{\partial^2}{\partial y^2} + 2e_{36}^0 \frac{\partial^2}{\partial x \partial y} \qquad (2)$$

where e_{31}^0, e_{32}^0, and e_{36}^0 are piezoelectric [(charge/area)/strain] constants. The above operator can be modified for use in polar coordinates by use of the chain rule from calculus. The function $F_k(\mathcal{P})$ accounts for the electrode coverage of the lamina and is defined by

$$F_k(\mathcal{P}) = \begin{cases} 1, & \text{if } (\mathcal{P}) \text{ is within the electrode coverage} \\ 0, & \text{otherwise} \end{cases}$$

The superscripts s or a that appear on $F_k(\mathcal{P})$ refer to laminae acting as sensors or actuators, respectively. For a rectangular plate, a and b are the respective length and width laminate; for a circular plate, a will denote the radius. In both cases, h is the total thickness of the laminate. The quantity $\bar{z}_k$ is the distance of the geometric center of the kth sensor to the midplane of the laminate, and N is the number of piezosensors. Figure 1 shows the coordinate axes and dimensions for a rectangular laminate with piezoelement coverage.

For a thin piezoelectric laminate with midplane symmetry and mechanically isotropic layers, the equation of motion for the transverse displacement that is caused by the converse piezoelectric effect alone is

$$D_E \nabla^4 w(\mathcal{P}, t) + \rho h \frac{\partial^2 w(\mathcal{P}, t)}{\partial t^2} = -\sum_{k \in M} h_k \bar{z}_k G_k(t) L_w \left[F^a(\mathcal{P}) P_0(\mathcal{P}) \right]_k \qquad (3)$$

where $\nabla^4 = \nabla^2 \nabla^2$, the biharmonic operator, whose form depends on the coordinate system $\mathcal{P}$ being used. This is known as the general

Received June 7, 1995; revision received Feb. 6, 1996; accepted for publication Feb. 22, 1996.

*Graduate Assistant, Department of Mechanical and Aerospace Engineering.
†Associate Professor, Department of Mechanical and Aerospace Engineering. Associate Fellow AIAA.

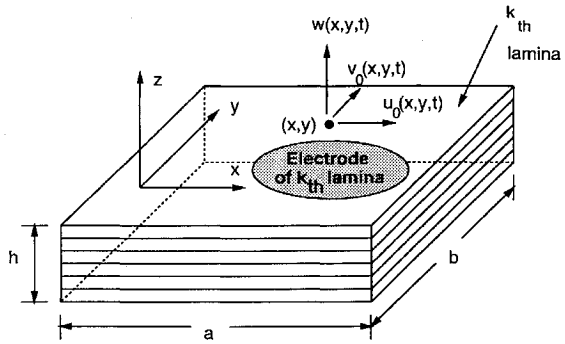

Fig. 1 Composite plate with surface electrode.

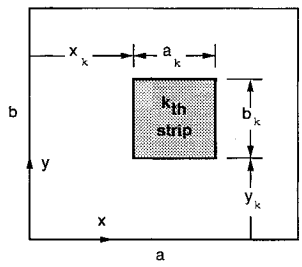

Fig. 2 Rectangular piezostrip dimensions for the plate.

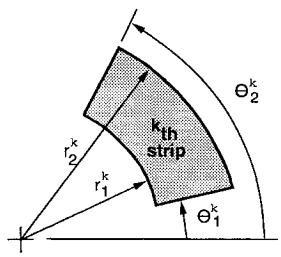

Fig. 3 Segmented strip suitable for the circular plate.

two-dimensional actuator equation. The quantities $G_k(t)$ are the charges applied to each of the M actuators. Here, D_E and ρh are the effective elastic bending modulus and mass/area of the laminate, respectively.

Because these piezofilms are so thin, they have very little global effect on structural mass and stiffness. Any discontinuities introduced by sensors and actuators that do not span the entire plate surface area are assumed to have a negligible effect on the applicability of thin piezoelectric laminate theory.

III. Charge/Modal Coordinate Relations

We consider cases where the boundary conditions permit mode orthogonalization. Rather than cut the piezoelements into complicated full patterns, which is a requirement for true modal sensors and actuators,[6] we place segmented strips at various locations on the plate, as shown in Figs. 2 and 3, similar to the approach in Ref. 10. From linear vibration theory for thin plates, the transverse deflection can be decomposed into its constituent modes according to

$$w(\mathcal{P}, t) = \sum_{j=1}^{\infty} w_j(\mathcal{P})\eta_j(t) \tag{4}$$

where $w_j(\mathcal{P})$ is the jth natural mode and $\eta_j(t)$ is its corresponding modal coordinate. For beams, the above modal expansion is a single summation; for thin plates, it becomes a double summation over the appropriate coordinate space. To reduce the double summation for plates to a single one, the modal coordinates can be arranged in a column vector. This allows the same analysis to be applied to beams and plates. Applying the modal expansion in Eq. (4) and orthogonality properties to Eqs. (1) and (3) results in the following expressions that relate piezoelement charges to modal displacements and vice versa[10]:

$$\{q(t)\} = [B^s]\{\eta(t)\} \tag{5}$$

$$\{\ddot{\eta}(t)\} + [\Lambda]\{\eta(t)\} = \{\mathcal{N}(t)\} = [B^a]^T\{hG(t)\} \tag{6}$$

where

$$B_{kj} = -\bar{z}_k \int\int_A \{F(\mathcal{P})P_0(\mathcal{P})L_w[w_j(\mathcal{P})]\}_k \, dA(\mathcal{P}) \tag{7}$$

and $\{\eta(t)\}$ denote the modal coordinates, $\{hG(t)\}$ are the electric potentials applied to the segmented actuators, and $\{\mathcal{N}(t)\}$ are the modal control inputs. The matrix $[\Lambda]$ is diagonal with $\Lambda_{ii} = \omega_i^2$ and ω_r is the vibration frequency of the rth mode. Note that $[B^s]$ and $[B^a]$ have order $(N \times \infty)$ and $(M \times \infty)$, respectively, and the entries of each depend on the number and size of the piezoelements. Because of the reciprocal nature of piezoelectric materials, the entries of $[B^s]$ and $[B^a]$ have the same form given by Eq. (7). If the kth element is changed from a sensor to an actuator, without changing its shape or location, then the entries for B^a_{kj} $(j = 1, \ldots, \infty)$ are the same as they were for a sensor, namely B^s_{kj}. To this end, note the difference between $[B^s]$ and $[B^a]$, because one may use segmented sensors and actuators that are different in size, location, and number. Equation (6) also results when other types of discrete actuators are used, so we can now use any of the previously developed modal control laws for such systems to suppress the elastic motion.

Note that the $[B]$ matrices are fully populated. For true modal sensors and actuators,[6] $[B]$ is diagonal. By avoiding complicated shape requirements, we sacrifice the ability to directly sense or influence individual modes. This problem is overcome when the piezosensor output is processed through modal observers.[1]

Simple rectangular shapes can be modeled by

$$F_k(x, y)P_{0,k}(x, y) = [H(x - x_k) - H(x - x_k - a_k)]$$
$$\times [H(y - y_k) - H(y - y_k - b_k)] \tag{8}$$

where $H(x)$ is the spatial Heaviside step function and the strip dimensions are shown in Fig. 2. For rectangular strips of the form shown in Fig. 2 on a rectangular plate, the charge/modal coordinate matrix has the form

$$B_{kj} = -\bar{z}_k \left\{ e^0_{31,k} \int_{y_k}^{y_k + b_k} \left[\frac{\partial w_j}{\partial x}\right]_{x_k}^{x_k + a_k} dy \right.$$
$$+ e^0_{32,k} \int_{x_k}^{x_k + a_k} \left[\frac{\partial w_j}{\partial y}\right]_{y_k}^{y_k + b_k} dx$$
$$\left. + 2e^0_{36,k}\left[[w_j]_{x_k}^{x_k + a_k}\right]_{y_k}^{y_k + a_k} \right\} \tag{9}$$

If we further assume that the transverse deflection has no y dependence, then the entries of $[B]$ for a beam simplify to

$$B_{kj} = -e^0_{31,k}\bar{z}_k b_k \left[\left.\frac{dw_j(x)}{dx}\right|_{x_k + a_k} - \left.\frac{dw_j(x)}{dx}\right|_{x_k}\right] \tag{10}$$

For circular plates, a uniform segmented strip with boundaries suitable for polar coordinates has the form

$$F_k(r, \theta)P_{0,k}(r, \theta) = \left[H\left(r - r_1^k\right) - H\left(r - r_2^k\right)\right]$$
$$\times \left[H\left(\theta - \theta_1^k\right) - H\left(\theta - \theta_2^k\right)\right] \tag{11}$$

Figure 3 shows the dimensions of the strip. For piezostrips of this type, the entries of $[B]$ can be found explicitly. One must be careful in sensor and actuator placement, however, because an ill-conditioned $[B]$ matrix may occur.[10] As shown later, the left-hand square portion of the charge/modal coodinate matrices must be invertible to extract modal information from the sensor output and to accomplish

vibration control using piezoactuators. When using strips of this form, the charge/modal coordinate matrix becomes

$$B_{kj} = -\bar{z}_k \int_{r_1^k}^{r_2^k} \int_{\theta_1^k}^{\theta_2^k} \left\{ \left(e^0_{31,k} \cos^2\theta + e^0_{32,k} \sin^2\theta + e^0_{36,k} \sin 2\theta\right) \times \frac{\partial^2 w_j}{\partial r^2} + \left(e^0_{31,k} \sin^2\theta + e^0_{32,k} \cos^2\theta - e^0_{36,k} \sin 2\theta\right) \times \left(\frac{1}{r}\frac{\partial w_j}{\partial r} + \frac{1}{r^2}\frac{\partial^2 w_j}{\partial \theta^2}\right) + 2\left(\frac{e^0_{32,k} - e^0_{31,k}}{2} \sin 2\theta + e^0_{36,k} \cos 2\theta\right) \frac{\partial}{\partial r}\left(\frac{1}{r}\frac{\partial w_j}{\partial \theta}\right) \right\}_k r \, \mathrm{d}r \mathrm{d}\theta \tag{12}$$

In the case where $e^0_{32} = e^0_{31}$ and $e^0_{36} = 0$ for all laminae,

$$B_{kj} = -\bar{z}_k e^0_{31,k} \left\{ \int_{\theta_1^k}^{\theta_2^k} \left[r \frac{\partial w_j}{\partial r} \right]_{r_1^k}^{r_2^k} \mathrm{d}\theta + \int_{r_1^k}^{r_2^k} \frac{1}{r} \left[\frac{\partial w_j}{\partial \theta} \right]_{\theta_1^k}^{\theta_2^k} \mathrm{d}r \right\} \tag{13}$$

If rectangular strips defined by Eq. (8) are used on the circular plate, one must implement Eq. (7) directly and resort to numerical integration techniques.[10]

IV. Modal Control

Several modal control laws have been developed in the past two decades that one can use on a system described by Eq. (6). In essence, modal control is based on selecting $\{hG(t)\}$ for each actuator such that the resulting modal force input will have the form

$$\{\mathcal{N}(t)\} = [G_1]\{\dot{\eta}(t)\} + [G_2]\{\eta(t)\} \tag{14}$$

in which $[G_1]$ and $[G_2]$ are control-gain matrices that are selected such that they minimize some performance index or lead to a desired set of closed-loop eigenvalues. In general, the entire infinity of the system modes cannot be controlled so that one bases the control-law design on a reduced set of modes, called the controlled modes. Selecting the number of modes we wish to control as C, we can write the modal equations of motion associated with the controlled set as

$$\{\ddot{\eta}_c(t)\} + [\Lambda_c]\{\eta_c(t)\} = [G_1]\{\dot{\eta}_c(t)\} + [G_2]\{\eta_c(t)\} = \left[B_c^a\right]^T \{hG(t)\} \tag{15}$$

where the subscript c denotes controlled modes. The matrices $[G_1]$ and $[G_2]$ are square with order $C \times C$ and $[B_c^a]$ has order $M \times C$.

The relationship between the number of controlled modes C and the number of actuators M is a critical factor in determining the control gains and influences the associated computational effort. One special case is encountered when the number of controlled modes is the same as the number of actuators, $M = C$. In that case, all coefficient matrices in Eq. (15) become square, and it is possible to design the controls for each mode independently of each other. This control design, which minimizes the computational effort and singularity problems associated with the control design, is referred to as independent modal-space control (IMSC).[11,12]

In past applications, where traditional point-force actuators, reaction wheels, or other types of torque actuators were envisioned as the input devices, implementation of IMSC was unrealistic in certain cases because of the substantial weight associated with the controllers. However, piezoelectric or piezoceramic actuators are extremely lightweight and therefore do not add any significant weight to the structure. Under the proposed configurations, one has little limitation in using as many actuators as the number of controlled modes.

In IMSC, one selects the modal-control inputs first and then specifies the actual input. For segmented piezoactuators, this is possible because the coefficient matrix $[B_c^a]$ is square. We can design the control action for each mode independently of the others, hence the name of the control law. We specify the control law to be of the form of Eq. (14) in which $[G_1]$ and $[G_2]$ are diagonal gain matrices selected such that each mode receives a desired level of damping or such that an optimality criterion is satisfied. The former approach is known as pole allocation. One can show that closed-form solutions to the control design exist both for the case of optimal control and when the closed-loop behavior of each mode is specified.[11,12]

The control design for pole allocation can be briefly summarized as follows: Selecting the gain matrices $[G_1]$ and $[G_2]$ as diagonal, with respective entries g_{1s} and g_{2s} ($s = 1, 2, \ldots, M$), we write the closed-loop modal equations as

$$\ddot{\eta}_s(t) + \omega_s^2 \eta_s(t) = g_{1s}\dot{\eta}_s(t) + g_{2s}\eta_s(t) \tag{16}$$

and select the gains such that the closed-loop poles have a desired form. The eigenvalue problem associated with each mode has the form

$$\lambda^2 - g_{1s}\lambda + \left(\omega_s^2 - g_{2s}\right) = 0$$

Prespecifying the desired closed-loop poles as

$$\lambda_s^{1,2} = \alpha_s \pm j\beta_s$$

leads to required gain selections

$$g_{1s} = 2\alpha_s, \qquad g_{2s} = -\left(\alpha_s^2 + \beta_s^2\right) + \omega_s^2$$

Once the modal-control gains are determined, the charges supplied to the segmented layers can be found by inverting Eq. (6):

$$\{hG(t)\} = \left[B_c^a\right]^{-T} \{\mathcal{N}(t)\} = \left[B_c^a\right]^{-T} \left([G_1]\{\dot{\eta}_c(t)\} + [G_2]\{\eta_c(t)\}\right) \tag{17}$$

V. Modal Coordinate and Velocity Extraction

Modal feedback control requires that the modal coordinates and velocities associated with the controlled modes be known. Depending on the types of sensors used, one has a variety of ways to extract modal information from the system output. We consider the use of piezoelectric sensors. The extraction of modal coordinates and velocities using segmented piezoelectric sensors is described in Ref. 1. We summarize the procedure.

If we partition $[B^s]$ into N modeled and $(\infty - N)$ residual portions, Eq. (5) becomes

$$\{q(t)\} = \begin{bmatrix} B_m^s & B_R^s \end{bmatrix} \begin{Bmatrix} \eta_m(t) \\ \eta_R(t) \end{Bmatrix} \tag{18}$$

Since there are only N strips, we can construct only N independent modal coordinate estimates at one time. We accomplish this by inverting $[B_m^s]$ and using

$$\{\hat{\eta}(t)\} = \left[B_m^s\right]^{-1} \{q(t)\} \tag{19}$$

Substituting Eq. (19) into Eq. (18) yields

$$\{\hat{\eta}(t)\} = \{\eta_m(t)\} + \left[B_m^s\right]^{-1} \left[B_R^s\right] \{\eta_R(t)\} \tag{20}$$

The measured modal coordinate $\hat{\eta}_r(t)$ is the true coordinate plus residual mode contamination.

We have extracted a modal coordinate measurement, but we still need a modal velocity, which we will obtain using modal observers.[13] The modal coordinates satisfy the uncoupled equations

$$\dot{\boldsymbol{x}}_r(t) = \begin{bmatrix} 0 & 1 \\ -\omega_r^2 & 0 \end{bmatrix} \boldsymbol{x}_r(t) + \begin{bmatrix} 0 \\ 1 \end{bmatrix} \mathcal{N}_r(t)$$
$$y_r(t) = [1 \quad 0] \boldsymbol{x}_r(t) \tag{21}$$

where $\boldsymbol{x}_r(t) = [\eta_r(t) \;\; \dot{\eta}_r(t)]^T$, $y_r(t) = \eta_r(t)$, and $\mathcal{N}_r(t)$ is the modal forcing for the rth mode. A full-order state estimator (observer) for Eq. (21) has the form[14]

$$\dot{z}_r(t) = \begin{bmatrix} -k_{r,1} & 1 \\ -\omega_r^2 - k_{r,2} & 0 \end{bmatrix} z_r(t) + \begin{bmatrix} k_{r,1} \\ k_{r,2} \end{bmatrix} \eta_r(t) + \begin{bmatrix} 0 \\ 1 \end{bmatrix} \mathcal{N}_r(t)$$

where $z_r(t) = [\tilde{\eta}_r(t)\ \dot{\tilde{\eta}}_r(t)]^T$ are the estimates for $\boldsymbol{x}_r(t)$. Closed-form expressions can be found for the gain matrix

$$\begin{bmatrix} k_{r,1} \\ k_{r,2} \end{bmatrix} = \begin{bmatrix} -(\lambda_1 + \lambda_2) \\ \lambda_1\lambda_2 - \omega_r^2 \end{bmatrix} \tag{22}$$

The entries of the gain matrix are chosen such that eigenvalues λ_1, λ_2 of the observer have negative real parts. For perfect measurements, $z(t) - x(t) \to 0$ as $t \to \infty$. Since the true modal coordinates are not known, the measurements $\hat{\eta}_r(t)$ are used to drive the modal observers. This is different from traditional Luenberger observers, in which one or more of the state variables is also the output. Here, the modal coordinate measurements are fed through the modal observers to estimate themselves, as well as modal velocities.

Also note that the above observer is for charge measurements. If the current is measured, a modal velocity measurement can be obtained, because electric current is the time derivative of charge. In this case, the modal observers can be used to estimate the modal coordinates.

The closed-loop control law that results when the modal observer outputs are used for beam control is the following:

$$\{\ddot{\eta}_c\} + [\Lambda_c]\{\eta_c\} = [G_1]\{\dot{\tilde{\eta}}\} + [G_2]\{\tilde{\eta}\} \tag{23}$$

$$\{\ddot{\eta}_R\} + [\Lambda_R]\{\eta_R\} = \left[B_R^a\right]^T\left[B_c^a\right]^{-T}([G_1]\{\dot{\tilde{\eta}}\} + [G_2]\{\tilde{\eta}\}) \tag{24}$$

According to Eq. (24), when $[B_R^a] \neq 0$, the residual modes are inadvertently excited when the control is applied. We have seen that as long as most of the lowest modes are included in the set of controlled modes, the excitation of the residual modes does not cause a problem.

To model noise, we assume that the charge is affected by some small quantity

$$\hat{q}_r(t) = q_r(t) + \epsilon_r, \qquad \epsilon_r = \Delta_r q_r(t) \tag{25}$$

in which Δ_r is a uniform random number. Noise modeled in this fashion further corrupts the modal coordinate measurements by coupling the observed modes.

In all real physical systems, there is some damping. Excluding a modal damping term or including an incorrect damping term in the observer equations makes the model unrealistic, but the modal observers inherently account for this by choice of the observer gains. If damping is modeled in the observers, then the observer gains can be shown to be[10]

$$\begin{bmatrix} k_{r,1} \\ k_{r,2} \end{bmatrix} = \begin{bmatrix} -(\lambda_1 + \lambda_2 + 2\zeta_r\omega_r) \\ \lambda_1\lambda_2 - \omega_r^2 + 2\zeta_r\omega_r(\lambda_1 + \lambda_2 + 2\zeta_r\omega_r) \end{bmatrix}$$

In comparison to Eq. (22), by including damping in the observer model, we require less gain for the same pole placement.

For very simple plate and beam geometries, closed-form solutions of the eigenvalue problem exist. In general, however, complicated geometries and boundary conditions do not permit such results. To analyze the effects of spatial discretization, we use the assumed-modes method.[15] For this approach, we choose a finite series of n twice-differentiable linearly independent admissible functions $\psi_j(x, y)$, which satisfy the geometric boundary conditions without overconstraining the problem. The mode-shape approximations $\phi_i(x, y)$ are then related to these functions by

$$\phi_i(x, y) = \sum_{j=1}^{n} U_{ji}\psi_j(x, y) \tag{26}$$

where the columns of the matrix U_{ij} are the normalized eigenvectors of the discrete eigenvalue problem resulting from the application of the assumed-modes method. Frequencies and charge/modal coordinate matrices computed using the mode approximations are denoted by $\tilde{\omega}$ and $[\tilde{B}]$, respectively.

VI. Structural Application

We have investigated the applicability of the control law [Eq. (14)] on beams and plates. Our initial results indicate that piezoceramics (lead zirconate titanates, or PZTs) do a better job of controlling the elastic motion than piezopolymer films (such as polyvinylidene fluoride, or PVDF). Although PVDF films are lighter and more flexible than PZT films, making it a more attractive material for sensors, piezoceramics have a higher coupling (d_{31}) between mechanical deformation and electric output than do PVDF films (see Table 1). This requires less energy to achieve the same control action. All numerical simulations in this paper used both segmented sensors and actuators that were made of either PZT or PVDF.

The required piezoelectric constants are calculated from

$$e_{31} = \frac{E_f}{1 - \nu_f^2}(d_{31} + \nu_f d_{32}), \qquad e_{32} = \frac{E_f}{1 - \nu_f^2}(\nu_f d_{31} + d_{32})$$

where the subscript f refers to the film mechanical properties. For beam analysis, only e_{31} needs to be considered. From Table 1, we see that its value for PZT is over 200 times larger than for PVDF. From Eq. (10), the entries of $[B]$ are directly proportional to e_{31}. Because the control law uses the inverse of this matrix, we therefore need 200 times more voltage to apply the same modal control, based on Eq. (17). This overshadows the fact that PVDF can take about 67 times more electric charge ($G_{\max}$) before the piezoelectric profile of the material breaks down.

When a charge is applied to the piezoactuators, distributed bending moments are induced. On the basis of linear piezoelectric laminate theory, they can be shown to be[9]

$$\begin{bmatrix} \mathcal{M}_1(x, t) \\ \mathcal{M}_2(x, t) \end{bmatrix} = \sum_{k \in M} \bar{z}_k h_k G_k(t) F_k(x, y) P_{0,k}(x, y) \begin{bmatrix} e_{31}^0 \\ e_{32}^0 \end{bmatrix}_k \tag{27}$$

Referring to the values in Table 1, it is seen that for a beam, a PZT actuator can apply up to three times more bending load than a PVDF actuator, given the same geometry.

The control we implemented was to make Eq. (16) behave as a second-order underdamped system. To achieve this, with a damping ratio ζ_s ($0 \leq \zeta_s \leq 1$), we set the control gains as

$$g_{1s} = -2\zeta_s\omega_s, \qquad g_{2s} = 0$$

Further, the modal velocity inputs will be those obtained from the sensor measurements after they have been processed through the modal observers, namely $\{\dot{\tilde{\eta}}(t)\}$. Hence, the modal control and applied electric fields are

$$\begin{aligned} \mathcal{N}_s(t) &= -2\zeta_s\omega_s\dot{\tilde{\eta}}_s(t) \\ G_r(t) &= -\frac{2}{h_{f,r}}\sum_{s=1}^{M}\left[B_c^a\right]_{sr}^{-1}\zeta_s\omega_s\dot{\tilde{\eta}}_s(t) \end{aligned} \tag{28}$$

It is evident from Eq. (28) that the thickness h_f of each piezoactuator limits the maximum electric field that can be applied.

To deal with the issues of maximum charge, we look at the maximum value of the charge for each actuator at each time step. We

Table 1 Typical properties of PZT and PVDF

Property	PZT G-1195	PVDF	Units
Young's modulus, E_f	63	3	GPa
d_{31}	179×10^{-12}	23×10^{-12}	C/N
d_{32}	179×10^{-12}	3×10^{-12}	C/N
Poisson's ratio, ν_f	1/3	1/3	none
e_{31}	16.92	0.081	C/m^2
e_{32}	16.92	0.036	C/m^2
Density, ρ_f	7.6	1.8	g/cm^3
$G_{\max}$	600×10^3	40×10^6	V/m

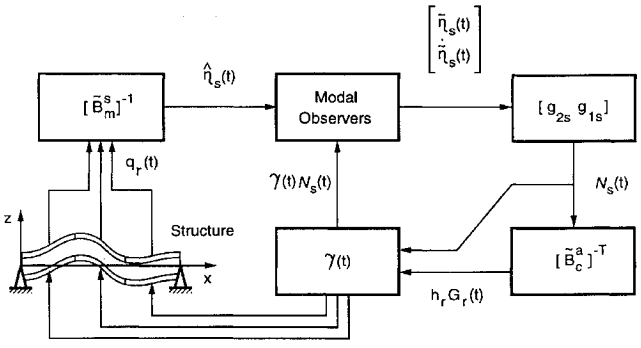

Fig. 4 Schematic of closed-loop control simulation.

compare the $G_i(t)$ $(i = 1, 2, \ldots, M)$ with their maximum allowable values and multiply the charge vector by a factor $\gamma(t)$ in which

$$\gamma(t) = \begin{cases} 1, & \text{if all } G_i \le G_i^{\max} \\ \min \left| \dfrac{G_i^{\max}}{G_i(t)} \right|, & \text{otherwise} \end{cases} \tag{29}$$

In essence, this scales all applied actuator voltages to the same effective damping ratio if any one actuator charge requirement is too large. Comparing Eqs. (29) and (28), the effective modal damping for this control scheme is then

$$\zeta(t) = \gamma(t)\zeta_{\text{des}}$$

where ζ_{des} is the desired level of modal damping. Using the natural mode approximations, the closed-loop equations of motion become

$$\{\ddot{\eta}_c(t)\} + [\Lambda_c]\{\eta_c(t)\} = \gamma(t)\left[B_c^a\right]^T\left[\tilde{B}_c^a\right]^{-T}([G_1]\{\dot{\tilde{\eta}}(t)\} + [G_2]\{\tilde{\eta}(t)\}) \tag{30}$$

$$\{\ddot{\eta}_R(t)\} + [\Lambda_R]\{\eta_R(t)\} = \gamma(t)\left[B_R^a\right]^T\left[\tilde{B}_c^a\right]^{-T}([G_1]\{\dot{\tilde{\eta}}(t)\} + [G_2]\{\tilde{\eta}(t)\}) \tag{31}$$

Figure 4 gives the proposed closed-loop control scheme using segmented piezosensors and piezoactuators.

VII. Closed-Loop Performance

We first apply the control law to rectangular plates. A simply supported plate is one case where the boundary conditions permit mode orthogonalization. For this case, a suitable modal expansion is given by[15]

$$w(x, y, t) = \sum_{l=1}^{\infty}\sum_{m=1}^{\infty} w_{lm}(x, y)\eta_{lm}(t)$$

with the normal modes and natural frequencies given by

$$w_s(x, y) = \frac{2}{\sqrt{\rho hab}} \sin\left(\frac{l_s\pi x}{a}\right)\sin\left(\frac{m_s\pi y}{b}\right)$$

$$\omega_s = \pi^2\left[\left(\frac{l_s}{a}\right)^2 + \left(\frac{m_s}{b}\right)^2\right]\sqrt{\frac{D_E}{\rho h}}$$

For this simulation, we modeled the first $n^2 = 100$ vibration modes for such a plate, and attempted to sense and control the 11, 12, 21, and 22 modes using the layout in Fig. 5. This layout was chosen to avoid any resemblance to sensor and actuator symmetry and/or collocation. Stainless steel ($E = 200$ GPa, $\nu = \frac{1}{3}$, $\rho = 7.8$ g/cm^3) was chosen as the shim material. The parameters for the rectangular-plate simulation are listed in Table 2. For each modal observer, the sampling rate was set to one-eighth of the vibration period of the mode with the highest frequency, ω_{22} in this case. The actuator inputs were computed according to Eq. (28) and updated at each sampling instant.

Table 2 Model parameters for rectangular-plate control simulation

Parameters	Rectangular plate	Sensors/actuators
Material	Steel	PZT/PVDF
Length	$a = 1$ m	See Fig. 5
Width	$b = 1.5a$	See Fig. 5
Thickness	$h_b = 5$ mm	$h_f = 0.1$ mm
Desired modal damping	$\zeta_{\text{des}} = 0.1$	
System modal damping	$\zeta_{\text{sys}} = 0.005$	
Modal observer poles	$\lambda_{1,2}^r = -10 \pm j\tilde{\omega}_r$ $(r = 1, \ldots, 4)$	
Measurement noise	$\Delta = [-0.05, 0.05]$	
Loading	Impulse, $\hat{F}_0 = 10$ N-s at $x/a = 0.4$, $y/b = 0.7$	

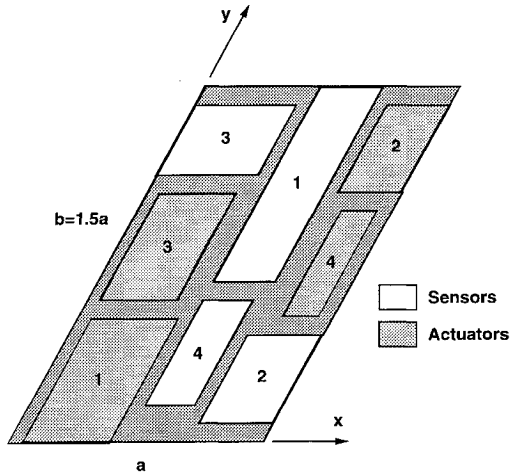

Fig. 5 Piezoelectric sensor/actuator layout for the rectangular plate simulation.

Figure 6 shows some results for the plate vibration control using PZT piezoelements. The closed-loop control system damps out the modal coordinates quicker than structural damping by itself. Referring to Fig. 6c, the effective damping does not immediately start at a minimum. This is because of the time taken for the modal observers to catch up to the system motion. Because of the control outlined in Eq. (29), each controlled mode experiences the same effective damping shown in Fig. 6c.

To compare the control capability of PZT vs PVDF, Fig. 7 shows the results when PVDF was substituted for PZT, with all other parameters unchanged. As the PZT results indicate, the closed-loop performance was still better than that in the uncontrolled system alone. The decrease in actuator weight, however, is traded for a doubling in the desired damping time. Not only do the PVDF actuators take longer to achieve the desired damping level than the PZTs, but, based on Figs. 6b and 7b, they also require a higher voltage (± 4000 V compared to ± 60 V). In real applications, this may be a short-circuit disaster waiting to happen.

To model decreasing piezoelement coverage on the rectangular plate, we introduce a parameter p $(0 \le p \le 1)$ and decrease the sensor and actuator coverage, as compared to that in Fig. 2, according to

$$x_r^* = x_r + [(1 + p)/2]a_r, \qquad a_r^* = pa_r$$

$$y_r^* = y_r + [(1 + p)/2]b_r, \qquad b_r^* = pb_r$$

The effects of decreasing sensor and actuator coverage can now be investigated. Here, we sensed the same $N^2 = 4$ modes as in the preceding plate case, using the parameters in Table 2. As performance indicators, two parameters were introduced: t_{thr}, the threshhold time required for all actuators to supply the desired damping level ζ_{des} and $\zeta_{\min}$, the minimum effective modal damping that was experienced by the system. Referring to the layout used in the preceding simulation, two cases are considered: 1) the sensor dimensions are unchanged and p^a is decreased, and 2) p^s and p^a are decreased by the same proportion.

Because both strip dimensions are scaled by p, the coverage area, relative to the original layout is proportional to $(p^s)^2$ for the sensors

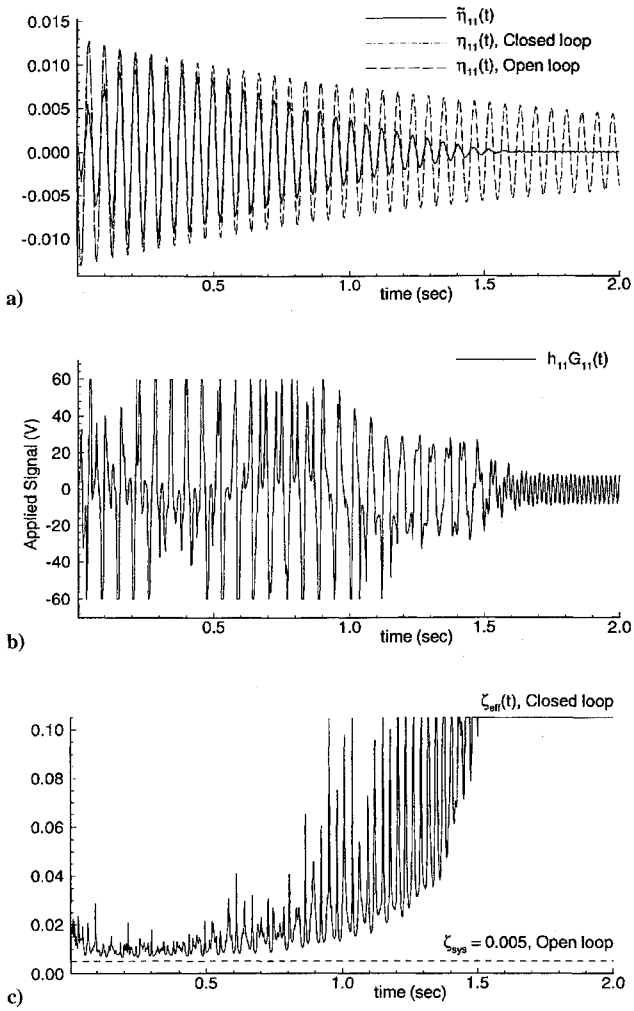

Fig. 6 Simulation results using PZT elements.

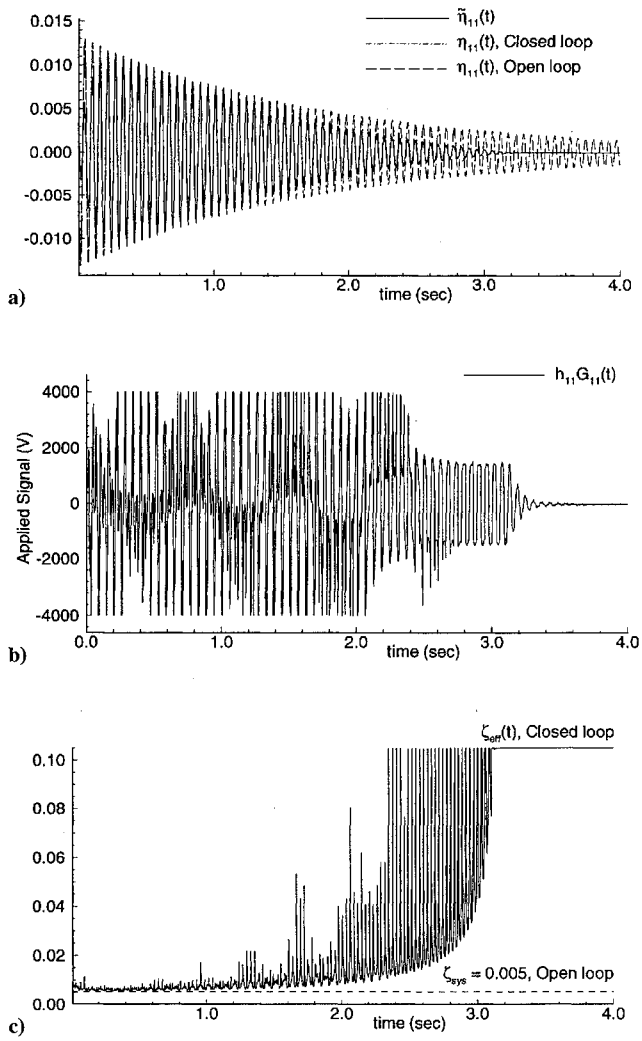

Fig. 7 Simulation results using PVDF elements.

and to $(p^a)^2$ for the actuators. Figure 8 shows the dependence of desired damping time and minimum effective modal damping on piezostrip coverage area using PZT sensors and actuators.

Referring to Fig. 8a, decreasing the sensor coverage had virtually no effect on the desired damping time t_{thr}. Although decreasing sensor coverage affects the quality of the modal observer output,[1] the finite charge allowance has a more significant effect on the control capability of piezofilms. Considering Fig. 8b, we see that decreasing sensor area has only a slight effect on $\zeta_{\min}$. This is because of the deterioration of the modal observer's performance with decreasing p^s.

Next, we consider circular plates. A circular plate clamped at its outer radius is another case where the natural modes are orthogonal. A convenient modal expansion for this case has the form[15]

$$w(r,\theta,t) = \sum_{m=1}^{\infty} w_{0m}(r)\eta_{0m}(t) + \sum_{l=1}^{\infty}\sum_{m=1}^{\infty}[w_{lmc}(r,\theta)\eta_{lmc}(t) + w_{lms}(r,\theta)\eta_{lms}(t)] \tag{32}$$

where

$$w_{0m}(r) = \frac{1}{\sqrt{2\pi\rho h a^2}}\left[\frac{J_0(\beta_{0m}r)}{J_0(\beta_{0m}a)} - \frac{I_0(\beta_{0m}r)}{I_0(\beta_{0m}a)}\right]$$

$$\left.\begin{matrix} w_{lmc}(r,\theta) \\ w_{lms}(r,\theta) \end{matrix}\right\} = \frac{1}{\sqrt{\pi\rho h a^2}}\left[\frac{J_l(\beta_{lm}r)}{J_l(\beta_{lm}a)} - \frac{I_l(\beta_{lm}r)}{I_l(\beta_{lm}a)}\right]\left\{\begin{matrix}\cos l\theta \\ \sin l\theta\end{matrix}\right.$$

$$(l, m = 1, 2, \ldots)$$

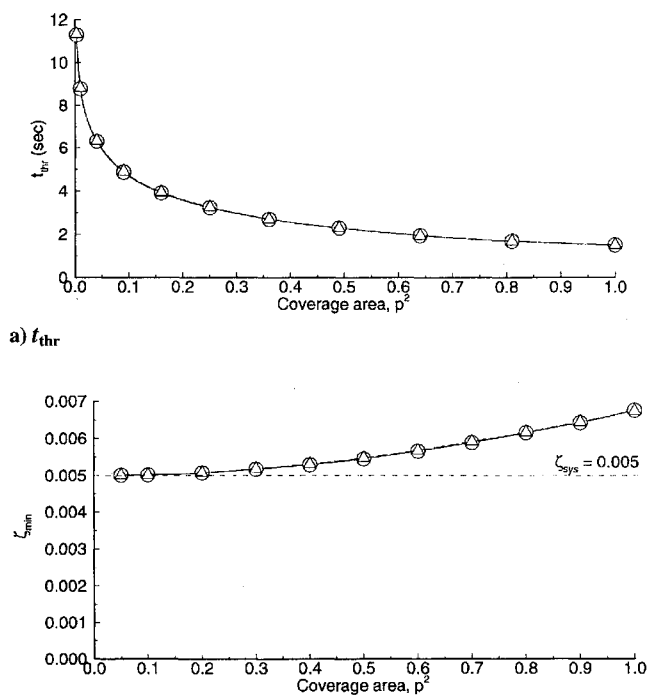

Fig. 8 Effect of plate PZT sensor/actuator coverage: ○, $p^s = 1$, vary p^a and △, vary both p^s and p^a by same amount.

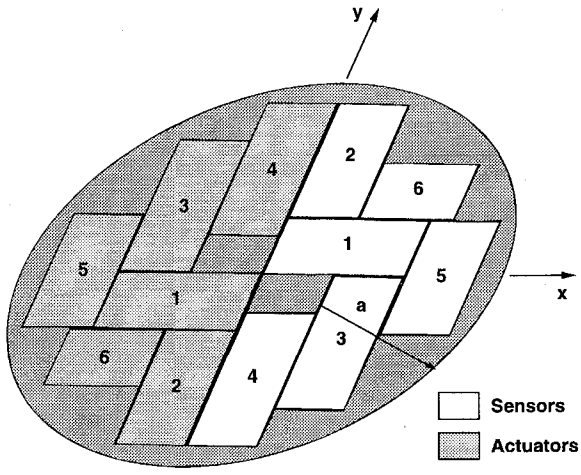

Fig. 9 Piezoelectric sensor/actuator layout for the circular plate simulation.

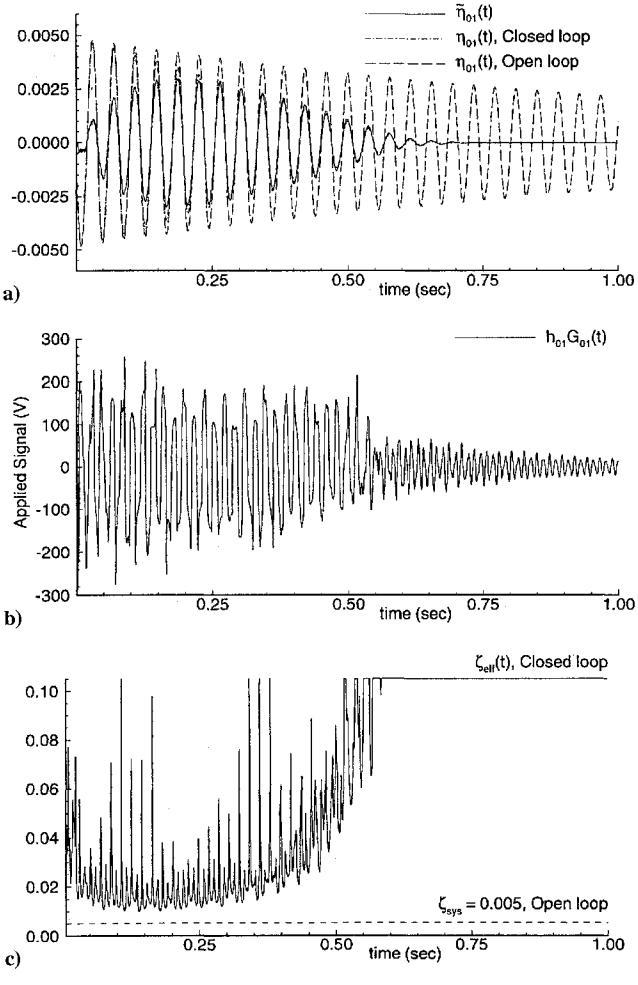

Fig. 10 Simulation results using PZT elements.

and J_l and I_l are Bessel and modified Bessel functions of the first kind and order l. Here, the eigenfunctions $w_{0m}(r)$ are the axisymmetric modes with unique frequencies ω_{0m}. For each frequency $\omega_{lm}(l > 0)$, however, there are two degenerate modes. Thus, any pair of modes that satisfy the boundary conditions and are orthogonal to each other will serve as suitable eigenfunctions. It is natural to select the sine $w_{lms}(r, \theta)$ and cosine $w_{lmc}(r, \theta)$ modes as this pair, because sine and cosine functions of the same argument are orthogonal to each other. The arguments $\beta_{lm}a$ satisfy the characteristic equation

$$I_l(\beta_{lm}a)J_{l-1}(\beta_{lm}a) - J_l(\beta_{lm}a)I_{l-1}(\beta_{lm}a) = 0$$

Table 3 Model parameters for the circular-plate control simulation.

Parameters	Circular plate	Sensors/actuators
Material	Steel	PZT
Radius	$a = 1$ m	See Fig. 9
Thickness	$h_b = 1$ cm	$h_f = 1$ mm
Desired modal damping	$\zeta_{des} = 0.1$	
System modal damping	$\zeta_{sys} = 0.005$	
Modal observer poles	$\lambda^r_{1,2} = -10 \pm j\omega_r$ $(r = 1, 2, \ldots, 6)$	
Measurement noise	$\Delta = [-0.05, 0.05]$	
Loading	Impulse, $\hat{F}_0 = 10$ N-s at $r/a = 0.25$, $\theta = -40$ deg	

which yields the corresponding natural frequencies

$$\omega_{lm} = (\beta_{lm}a)^2\sqrt{\left(D_E/\rho h a^4\right)}$$

For the simulation, we modeled the first 190 modes and attempted to sense and control the 01, 02, 11c, 11s, 12c, and 12s modes. For this case, we used the layout in Fig. 9 with the system parameters given in Table 3. Note that the actuator layout is simply the sensor arrangement rotated by 180 deg. The piezoelement layouts for a circular plate cannot be chosen as arbitrarily as for the rectangular plate. Sensors and actuators must be placed more carefully in this case because of the presence of degenerate modes. In comparison to the rectangular-plate case, we found that a faster observer sampling rate was necessary to achieve comparable control on the circular plate. This is also because of the closer spacing of the natural frequencies of the system. Here, we chose the rate to be 1/20 of the vibration period for ω_{12c}, the highest frequency in this case. Figure 10 shows the results for the fundamental mode of the clamped circular plate. Once again, the actuators help to damp out the vibration quicker than the structural damping alone.

VIII. Conclusions

We have presented a method to sense and control structural vibration by combining piezoelectric film technology with well-known modal control techniques. Segmented piezopolymer (PVDF) and piezoceramic (PZT) sensors and actuators together with modal observers make it feasible to apply modal control without substantially increasing the weight and stiffness of the structure to which they are applied.

Given the same dimensions, piezoceramic (PZT) actuators are more attractive than piezopolymer (PVDF) actuators for control, based on their ability to supply a specified damping level in a shorter time interval with significantly less energy. From a mechanical viewpoint, however, PVDF films make more attractive sensors than PZTs because they are lighter, tougher, and more flexible. Thus, depending on the application, one material may be more suitable than the other.

Although the time required to achieve a desired damping level increases with decreasing sensor/actuator coverage, good results are achieved even with relatively small sensor and actuator coverage. Although piezoelectric actuators may not always supply a desired loading because of a finite charge tolerance, what little they can do is far better than relying on structural damping alone.

Acknowledgments

This research was supported by the U.S. Federal Aviation Administration. The authors would like to thank Peter Shyprykevich, their Technical Monitor, for his helpful comments and suggestions.

References

[1]Callahan, J., and Baruh, H., "Modal Analysis Using Segmented Piezoelectric Sensors," *AIAA Journal*, Vol. 33, No. 12, 1995, pp. 2371–2378.

[2]Collins, S. A., Padilla, C. E., Notestine, R. J., von Flotow, A. H., Schmitz, E., and Ramey, M., "Design, Manufacture, and Application to Space Robotics of Distributed Piezoelectric Sensors," *Journal of Guidance, Control, and Dynamics*, Vol. 15, No. 2, 1992, pp. 396–403.

[3]Crawley, E. F., and de Luis, J., "Use of Piezoelectric Actuators as Elements of Intelligent Structures," *AIAA Journal*, Vol. 25, No. 10, 1987, pp. 1373–1385.

[4]Crawley, E. F., and de Luis, J., "Experimental Verification of Distributed Piezoelectric Actuators for Use in Precision Space Structures," *Proceedings of the AIAA 27th Structural Dynamics Conference*, AIAA, New York, 1986, pp. 116–124.

[5]Hanagud, S., Obal, M. W., and Calise, A. J., "Optimal Vibration Control by the Use of Piezoceramic Sensors and Actuators," *Journal of Guidance, Control, and Dynamics*, Vol. 15, No. 5, 1992, pp. 1199–1206.

[6]Lee, C.-K., and Moon, F. C., "Modal Sensors/Actuators," *Journal of Applied Mechanics*, Vol. 57, June 1990, pp. 434–441.

[7]Tzou, H.-S., and Fu, H. Q., "A Study on Segmentation of Distributed Piezoelectric Sensors and Actuators: Part 1—Theoretical Analysis," *Journal of Sound and Vibration*, Vol. 172, No. 2, 1994, pp. 247–260.

[8]Tzou, H.-S., and Fu, H. Q., "A Study on Segmentation of Distributed Piezoelectric Sensors and Actuators: Part 2—Parametric Study and Active Vibration Controls," *Journal of Sound and Vibration*, Vol. 172, No. 2, 1994, pp. 261–276.

[9]Lee, C.-K., "Theory of Laminated Piezoelectric Plates for the Design of Distributed Sensors/Actuators. Part I: Governing Equations and Reciprocal Relationships," *Journal of the Acoustical Society of America*, Vol. 87, No. 3, 1990, pp. 1144–1158.

[10]Callahan, J., "Modal Analysis and Control of Flexible Bodies Using Segmented Piezoelectric Components," M.S. Thesis, Dept. of Mechanical and Aerospace Engineering, Rutgers Univ., New Brunswick, NJ, Jan. 1995.

[11]Oz, H., and Meirovitch, L., "Optimal Modal Space Control of Flexible Gyroscopic Systems," *Journal of Guidance and Control*, Vol. 3, No. 3, 1980, pp. 218–226.

[12]Meirovitch, L., and Baruh, H., "Control of Self-Adjoint Distributed Parameter Systems," *Journal of Guidance, Control, and Dynamics*, Vol. 5, No. 1, 1982, pp. 60–66.

[13]Choe, K., and Baruh, H., "Sensor Failure Detection in Flexible Structures Using Modal Observers," *Journal of Dynamic Systems, Measurement and Control*, Vol. 115, No. 3, 1993, pp. 411–418.

[14]Chen, C.-T., *Linear System Theory and Design*, Holt, Rinehart, and Winston, Philadelphia, 1984, Chap. 7.

[15]Meirovitch, L., *Analytical Methods in Vibrations*, Macmillan, New York, 1967, Chap. 5.